

1 **Intelligible speech synthesis from neural decoding of spoken sentences**

2 **Authors** Gopala K. Anumanchipalli^{1,2*}, Josh Chartier^{1,2,3*}, Edward F. Chang^{1,2,3}

3 * Authors contributed equally

4

5 **Affiliations**

6 ¹Departments of Neurological Surgery and Physiology, University of California–San
7 Francisco, San Francisco, California 94143, USA

8 ²Weill Institute for Neurosciences, University of California–San Francisco, San
9 Francisco, California 94158, USA

10 ³University of California–Berkeley and University of California–San Francisco Joint
11 Program in Bioengineering, Berkeley, California 94720, USA

12

13 Correspondence and requests for materials should be addressed to

14 Edward.Chang@ucsf.edu

15 The authors declare no competing interests.

16

17 **Abstract**

18 The ability to read out, or decode, mental content from brain activity has significant
19 practical and scientific implications¹. For example, technology that translates cortical
20 activity into speech would be transformative for people unable to communicate as a result
21 of neurological impairment^{2,3,4}. Decoding speech from neural activity is challenging
22 because speaking requires extremely precise and dynamic control of multiple vocal tract
23 articulators on the order of milliseconds. Here, we designed a neural decoder that
24 explicitly leverages the continuous kinematic and sound representations encoded in
25 cortical activity^{5,6} to generate fluent and intelligible speech. A recurrent neural network
26 first decoded vocal tract physiological signals from direct cortical recordings, and then
27 transformed them to acoustic speech output. Robust decoding performance was achieved
28 with as little as 25 minutes of training data. Naïve listeners were able to accurately

29 identify these decoded sentences. Additionally, speech decoding was not only effective
30 for audibly produced speech, but also when participants silently mimed speech. These
31 results advance the development of speech neuroprosthetic technology to restore spoken
32 communication in patients with disabling neurological disorders.

33

34 **Text**

35 Neurological conditions that result in the loss of communication are devastating.
36 Many patients rely on alternative communication devices that measure residual nonverbal
37 movements of the head or eyes⁷, or even direct brain activity^{8,9}, to control a cursor to
38 select letters one-by-one to spell out words. While these systems dramatically enhance a
39 patient's quality of life, most users struggle to transmit more than 10 words/minute¹⁰, a
40 rate far slower than the average of 150 words/min in natural speech. A major hurdle is
41 how to overcome the constraints of current spelling-based approaches to enable far higher
42 communication rates.

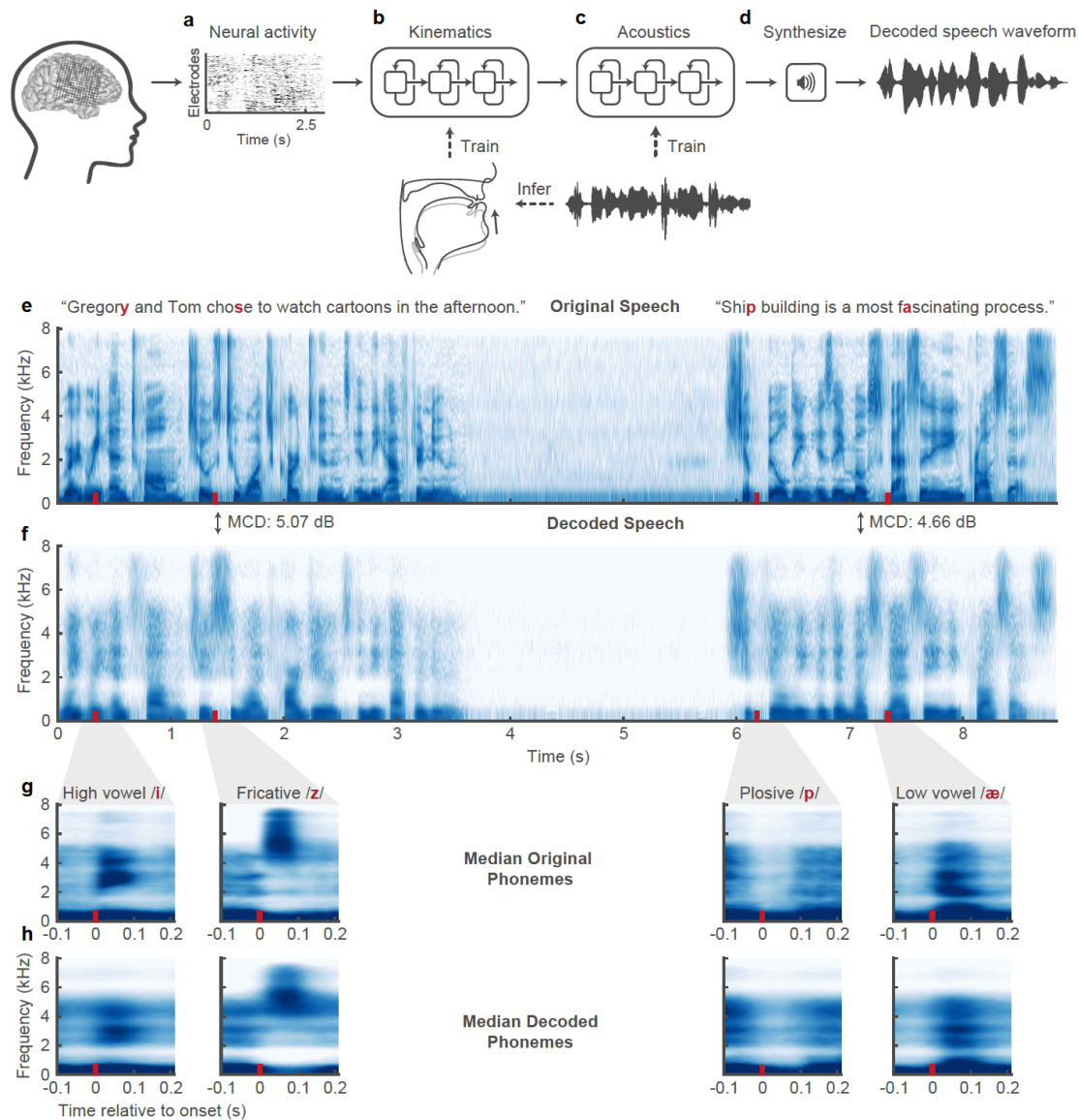
43 A promising alternative to spelling-based approaches is to directly synthesize
44 speech^{11,12}. Spelling is a sequential concatenation of discrete letters, whereas speech is
45 produced from a fluid stream of overlapping, multi-articulator vocal tract movements¹³.
46 For this reason, a biomimetic approach that focuses on vocal tract movements and the
47 sounds they produce may be the only means to achieve the high communication rates of
48 natural speech, and likely the most intuitive for users to learn^{14,15}. In patients with
49 paralysis, for example from ALS or brainstem stroke, high fidelity speech control signals
50 may only be accessed by directly recording from intact cortical networks using a brain-
51 computer interface.

52 Our goal was to demonstrate the feasibility of a neural speech prosthetic by
53 translating brain signals into intelligible synthesized speech at the rate of a fluent speaker.
54 To accomplish this, we recorded high-density electrocorticography (ECoG) signals from
55 three participants undergoing intracranial monitoring for epilepsy treatment as they spoke
56 several hundred sentences aloud. We designed a recurrent neural network that decoded
57 cortical signals with an explicit intermediate representation of the articulatory dynamics
58 to generate audible speech.

59 An overview of our two-stage decoder approach is shown in Figure 1a-d. In the
60 first stage, a bidirectional long short term memory (bLSTM) recurrent neural network¹⁶
61 decodes articulatory kinematic features from continuous neural activity (Figure 1a, b). In
62 the second stage, a separate bLSTM decodes acoustic features from the decoded
63 articulatory features from stage 1 (Figure 1c). The audio signal is then synthesized from
64 the decoded acoustic features (Figure 1d).

65 There are three sources of data for training the decoder: high density ECoG
66 recordings, acoustics, and articulatory kinematics. For ECoG, high-gamma amplitude
67 envelope (70-200 Hz)¹⁷, and low frequency component (1-30 Hz)¹⁸ were extracted from
68 the raw signal of each electrode. Electrodes were selected if they were located on key
69 cortical areas for speech: ventral sensorimotor cortex (vSMC)¹⁹, superior temporal gyrus
70 (STG)²⁰, or inferior frontal gyrus (IFG)²¹ (Figure 1a). For acoustics, instead of a typical
71 spectrogram, we used 25 mel-frequency cepstral coefficients (MFCCs), 5 sub-band
72 voicing strengths for glottal excitation modelling, pitch, and voicing (32 features in all).
73 These acoustic parameters are specifically designed to emphasize perceptually relevant
74 acoustic features while maximizing audio reconstruction quality²².

75 Lastly, a key component of our decoder is an intermediate articulatory kinematic
76 representation between neural activity and acoustics (Figure 1b). Our previous work
77 demonstrated that articulatory kinematics is the predominant representation in the
78 vSMC⁶. Since it was not possible to record articulatory movements synchronously with
79 neural recordings, we used a statistical speaker-independent Acoustic-to-Articulatory
80 inversion method to estimate vocal tract kinematic trajectories corresponding to the
81 participant's produced speech acoustics. We added additional physiological features (e.g.
82 manner of articulation) to complement the kinematics and optimized these values within
83 a speech autoencoder to infer the full intermediate articulatory kinematic representation
84 that captures vocal tract physiology during speech production (see methods). From these
85 features, it was possible to accurately reconstruct the speech spectrogram (Figure 1e,f).



86

87 **Figure 1: Speech synthesis from neurally decoded spoken sentences.** **a**, The neural
 88 decoding process begins by extracting high-gamma amplitude (70-200Hz) and low-
 89 frequency (1-30Hz) ECoG activity. **b**, A 3-layer bi-directional long short term memory
 90 (bLSTM) neural network learns to decode kinematic representations of articulation from
 91 filtered ECoG signals. **c**, An additional 3-layer bLSTM learns to decode acoustics from
 92 the previously decoded kinematics. Acoustics are represented as spectral features (e.g.
 93 Mel-frequency cepstral coefficients (MFCCs)) extracted from the speech waveform. **d**,
 94 Decoded signals are synthesized into an acoustic waveform. **e**, Spectrogram shows the
 95 frequency content of two sentences spoken by a participant. **f**, Spectrogram of
 96 synthesized speech from brain signals recorded simultaneously with the speech in **e**. Mel-
 97 cepstral distortion (MCD), a metric for assessing the spectral distortion between two
 98 audio signals, was computed for each sentence between the original and decoded audio.
 99 **g,h** 300 ms long, median spectrograms that were time-locked to the acoustic onset of
 100 phonemes from original (**g**) and decoded (**h**) audio. Medians were computed from

101 phonemes in 100 sentences that were withheld during decoder training (n: /i/ = 112, /z/ =
102 115, /p/ 69, /ae/ = 86). These phonemes represent the diversity of spectral features.
103 Original and decoded median phoneme spectrograms were well correlated ($r > 0.9$ for all
104 phonemes, $p=1e-18$)
105

106 *Synthesis performance*

107 Overall, we observed highly detailed reconstructions of speech decoded from
108 neural activity alone (See supplemental video). Examples of decoding performance are
109 shown in Figure 1 (e,f), where the audio spectrograms from two original spoken
110 sentences are plotted above those decoded from brain activity. The first sentence is
111 representative of the median performance and the second shows one of the best decoded
112 sentences. The decoded spectrogram contained salient energy patterns present in the
113 original spectrogram.

114 To illustrate the quality of reconstruction at the phonetic level, we compared
115 median spectrograms of phonemes from original and decoded audio. As shown in Figure
116 1 g,h, the formant frequencies (F1-F3, seen as high energy resonant bands in the
117 spectrograms) and distribution of spectral energy for high and low vowels (/i/ and /ae/,
118 respectively) of the decoded examples closely resembled the original speech. For alveolar
119 fricatives (/z/) the high frequency (>4kHz) acoustic energy was well represented in both
120 spectrograms. For plosives (/p/), the short pause (relative silence during the closure)
121 followed by a broadband burst of energy (after the release) was also well decoded. The
122 decoder also correctly reconstructed the silence in between the sentences when the
123 participant was not speaking.

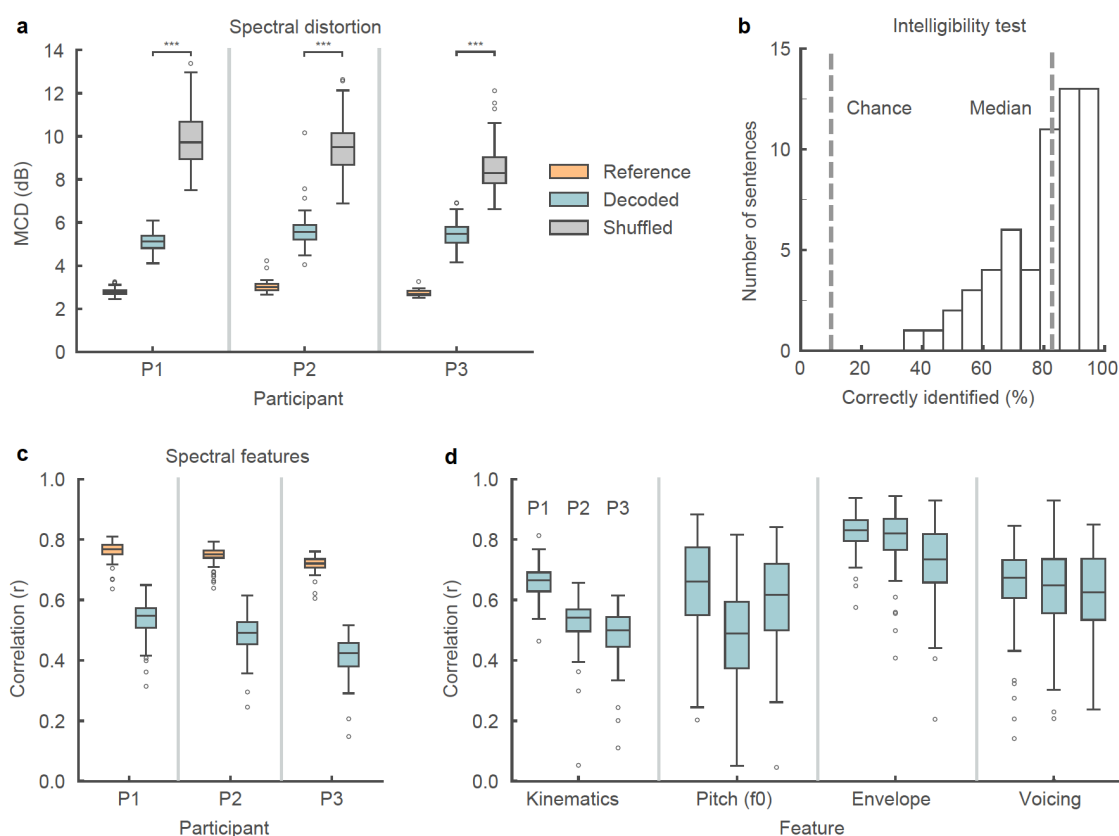
124 To quantify performance, we tested the neural decoder for each participant on 100
125 sentences that were withheld during the training and optimization of the full model. In

126 traditional speech synthesis, the spectral distortion of synthesized speech from ground-
127 truth is commonly reported using the mean Mel-Cepstral Distortion (MCD)²³. The use of
128 Mel-Frequency bands emphasizes the distortion of perceptually relevant frequency bands
129 of the audio spectrogram²⁴. In Figure 2a, the MCD of neurally decoded speech was
130 compared with reference synthesis from articulatory kinematics and chance-level
131 decoding (lower MCD is better). The reference synthesis acts as a bound for performance
132 as it simulated what perfect neural decoding of the kinematics would achieve. For our
133 participants (P1, P2, P3), the median MCD scores of decoding speech were 5.14 dB, 5.55
134 dB, and 5.49 dB, all better than chance-level decoding ($p < 1e-18$, $n=100$ sentences,
135 Wilcoxon signed-rank test (WSRT), for each participant). These scores were on par with
136 state-of-the-art approaches to decode speech from facial surface electromyography
137 (EMG) with similarly sized datasets (average MCD of 5.21 dB)²⁵.

138 To assess the perceptual intelligibility of the decoded speech, we used Amazon
139 Mechanical Turk to evaluate naïve listeners' ability to understand the neurally decoded
140 trials. We asked 166 people to identify which of 10 sentences (written on screen)
141 corresponded to the decoded audio they heard. The median percentage of participants
142 who correctly identified each sentence was 83%, significantly above chance (10%)
143 (Figure 2b).

144 In addition to spectral distortion and intelligibility, we also examined the
145 correlations between original and decoded spectral features. The median correlations (of
146 sentences, Pearson's r) of the mean decoded spectral feature (pitch + 25 MFCCs +
147 excitation strengths + voicing) for each participant were 0.55, 0.49, and 0.42 (Figure 2c).
148 Similarly, for decoded kinematics (the intermediate representation), the median

149 correlations were 0.66, 0.54, and 0.50 (Figure 2d). Finally, we examined three key
 150 aspects of prosody for intelligible speech: pitch (f_0), speech envelope, and voicing²⁶
 151 (Figure 2d). For all participants, these features were decoded well above chance-level
 152 correlations ($r > 0.6$, except f_0 for P2: $r = 0.49$, $p < 1e-10$, $n = 100$, WSRT, for all
 153 participants and features in Figure 2c-d). Correlation decoding performance for all other
 154 features is shown in Extended Data Figure 1a,b.



155

156 **Figure 2: Decoded speech intelligibility and feature-specific performance.. a,**
 157 Spectral distortion, measured by Mel-Cepstral Distortion (MCD) (lower values are
 158 better), between original spoken sentences and neurally decoded sentences that were held
 159 out from model training ($n = 100$). Reference MCD refers to the MCD resulting from the
 160 synthesis of original kinematics without neural decoding and provides an upper bound for
 161 performance. MCD scores were compared to chance-level MCD scores obtained by
 162 shuffling data before decoding. **b,** Decoded sentence intelligibility was assessed by
 163 asking naïve participants to identify the sentence they heard from 10 choices. Each
 164 sample ($n = 60$) represents the percentage of correctly identified trials for one sentence.
 165 The median sentence was correctly identified 83% of the time. **c,** Correlation of original

166 and decoded spectral features. Values represent the mean correlation of the 32 spectral
167 features for each sentence ($n = 100$). Correlation performance for individual spectral
168 features is reported in extended data figure 1b. **d**, Correlations between original and
169 decoded intelligibility-relevant features. Kinematic values represent the mean correlation
170 of the 33 kinematic features (the intermediate representation) for each sentence ($n = 100$).
171 Correlation performance for individual kinematic features is reported in extended data
172 figure 1a. Box plots depict median (horizontal line inside box), 25th and 75th percentiles
173 (box), 25/75th percentiles $\pm 1.5 \times$ interquartile range (whiskers), and outliers (circles).
174 Distributions were compared with each as other as indicated or with chance-level
175 distributions using two-tailed Wilcoxon signed-rank tests ($p < 1e-10$, $n = 100$, for all
176 tests).
177

178

179 *Effects of model design decisions*

180 The following analyses were performed on data from P1. In designing a neural
181 decoder for clinical applications, there are several key considerations regarding the input
182 to the model. First, in patients with severe paralysis or limited speech ability, training
183 data may be very difficult to obtain. In audio-based commercial applications like digital
184 assistants, successful speech synthesis from text relies on tens of hours of speech²⁷.
185 Despite having limited neural data, we observed high decoding performance, and
186 therefore we wanted to assess how much data was necessary to achieve this level of
187 performance. Furthermore, we wanted to see if there was a clear advantage in explicitly
188 modeling articulatory kinematics as an intermediate step over decoding acoustics directly
189 from the ECoG signals. The motivation for including articulatory kinematics was to
190 reduce the complexity of the ECoG-to-acoustic mapping because it captures the
191 physiological process by which speech is generated and is encoded in the vSMC⁶.

192 We found robust performance could be achieved with as little as 25 minutes of
193 speech, but performance continued to improve with the addition of more data (Figure
194 3a,b). A crucial factor in performance was the articulatory intermediate training step.

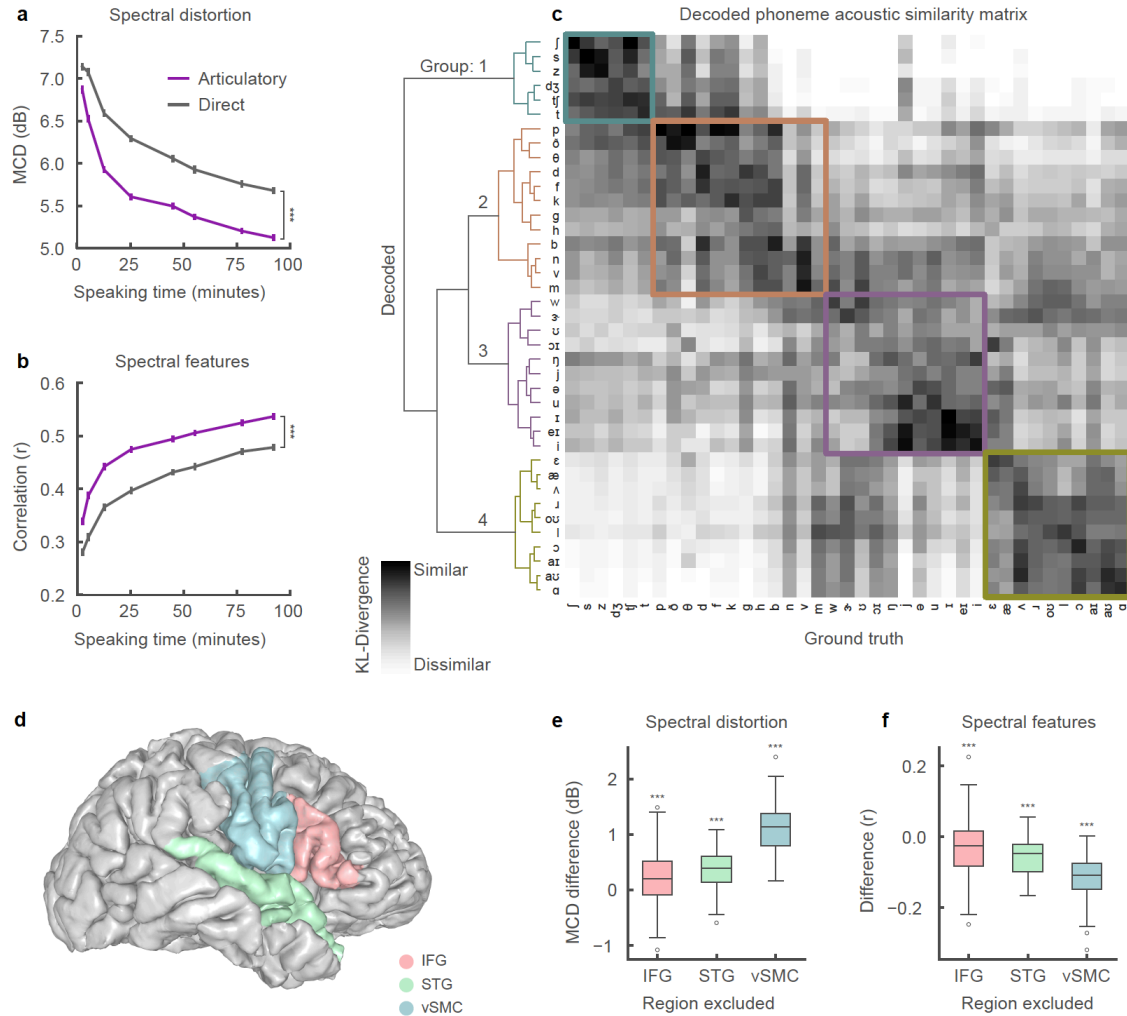
195 Without this step, direct ECoG to acoustic decoding MCD was offset by 0.54 dB using
196 the full data set (Figure 3a) ($p=1e-17$, $n=100$, WSRT), a substantial difference given that
197 a change in MCD as small as 0.2 dB is perceptually noticeable²⁸. While the two
198 approaches might perform comparably with enough data, the biomimetic approach using
199 an intermediate articulatory representation is superior because it requires less training
200 data.

201 Second, we wanted to understand the acoustic-phonetic properties that were
202 preserved in decoded speech because they are important for relative phonetic
203 discrimination. To do this, we compared the acoustic properties of decoded phonemes to
204 ground truth by constructing a statistical distribution of the spectral feature vectors for
205 each phoneme. Using Kullback-Leibler (KL) divergence, we compared the distribution of
206 each decoded phoneme to the distribution of each ground-truth phoneme to determine
207 how similar they were (Figure 3c). From the acoustic similarity matrix of only ground-
208 truth phoneme-pairs (Extended Data Figure 2), we expected that, in addition to the same
209 decoded and ground-truth phoneme being similar to one another, phonemes with shared
210 acoustic properties would also be characterized as similar to one another. For example,
211 two fricatives will be more acoustically similar to one another than to a vowel.

212 Hierarchical clustering on the KL-divergence of each phoneme pair demonstrated
213 that phonemes were clustered into four main groups. These groups represent the primary
214 decoded acoustic differences between phonemes. Within each group, phonemes were
215 more likely to be confused with one another due to their shared acoustic properties. For
216 instance, a decoded /s/ may easily be confused with /z/ or other phonemes in Group 1.
217 Group 1 contained consonants with an alveolar place of constriction. Group 2 contained

218 almost all other consonants. Group 3 contained mostly high vowels. Group 4 contained
219 mostly mid and low vowels. The difference between groups tended to correspond to
220 variations along acoustically significant dimensions (frequency range of spectral energy
221 for consonants, and formants for vowels). These groupings were similar to those obtained
222 by clustering KL-divergence of ground-truth phoneme pairs (Extended Data Figure 2).

223 Third, since the success of the decoder depends on the initial electrode placement,
224 we wanted to assess how much the cortical activity of each brain region contributed to
225 decoder performance. We quantified the contributions of the vSMC, STG, and IFG by
226 training decoders in a leave-one-region-out fashion and comparing performance (Figure
227 3d). Removing any region led to decreased decoder performance (Figure 3e-f) ($p < 3e-4$,
228 $n=100$, WSRT). However, excluding vSMC resulted in the largest decrease in
229 performance (1.13 dB MCD increase).



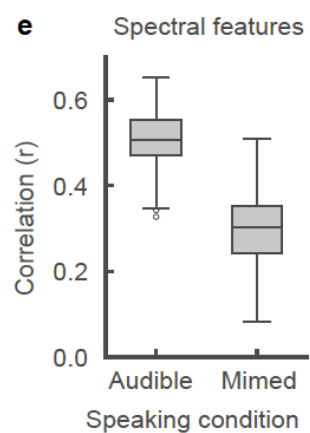
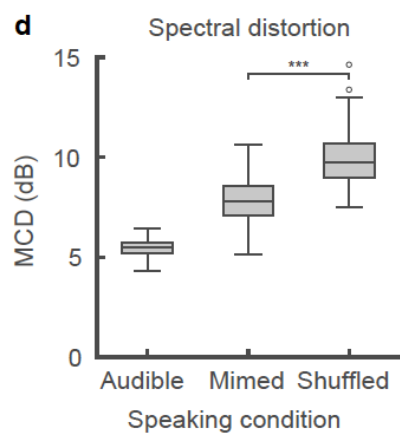
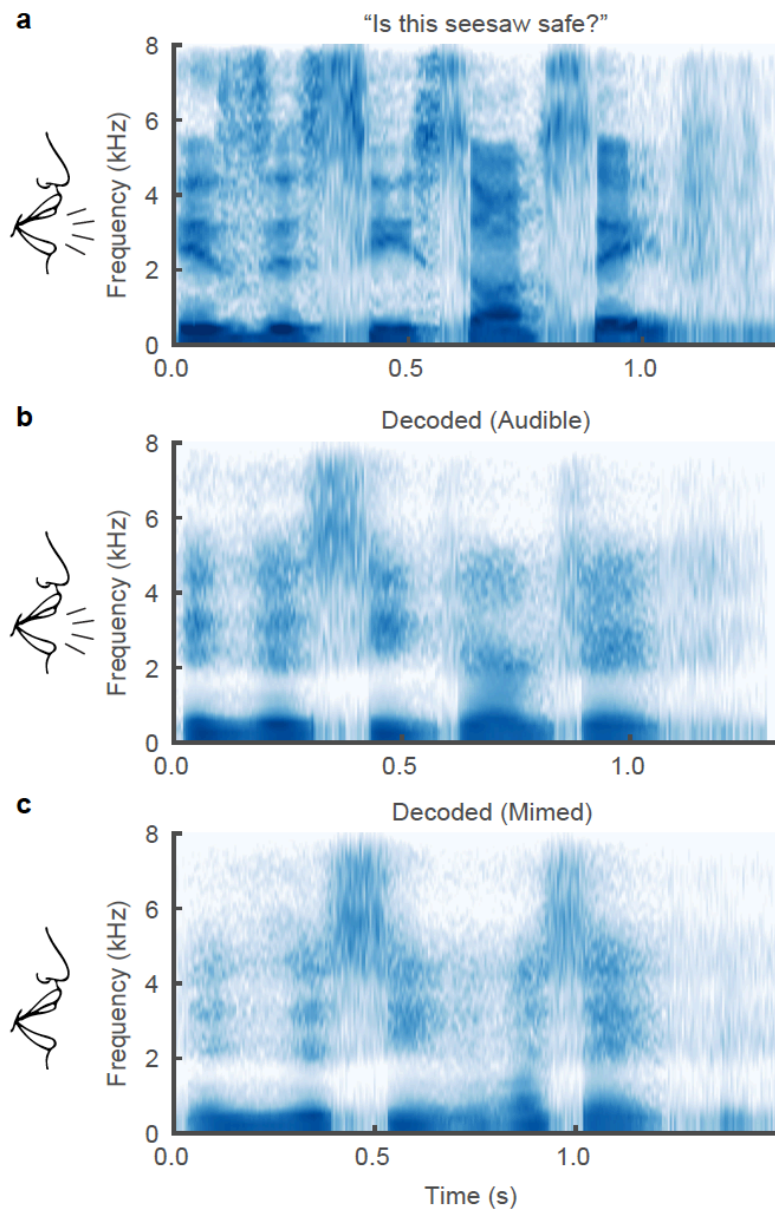
230

231 **Figure 3: Effects of model design decisions.** **a, b**, Mean correlation of original and
 232 decoded spectral features (**a**) and mean spectral distortion (MCD) (**b**) for model trained
 233 on varying amounts of training data. Training data was split according to recording
 234 session boundaries resulting the following sizes: 2.4, 5.2, 12.6, 25.3, 44.9, 55.2, 77.4, and
 235 92.3 minutes of speaking data. The neural decoding approach that included an
 236 articulatory intermediate stage (purple) performed significantly better with every size of
 237 training data than direct ECoG to acoustics decoder (grey) (all: $p < 1e-5$, $n = 100$;
 238 Wilcoxon signed-rank test, error bars = SE). **c**, Acoustic similarity matrix compares
 239 acoustic properties of decoded phonemes and originally spoken phonemes. Similarity is
 240 computed by first estimating a gaussian kernel density for each phoneme (both decoded
 241 and original) and then computing the Kullback-Leibler (KL) divergence between a pair of
 242 decoded and original phoneme distributions. Each row compares the acoustic properties
 243 of a decoded phoneme with originally spoken phonemes (columns). Hierarchical
 244 clustering was performed on the resulting similarity matrix. **d**, Anatomical reconstruction
 245 of a single participant's brain with the following regions used for neural decoding:
 246 ventral sensorimotor cortex (vSMC), superior temporal gyrus (STG), and inferior frontal
 247 gyrus (IFG). **e, f**, Difference in spectral distortion (MCD) (**e**), and difference in

248 correlation (Pearson's r) performance (**f**) between decoder trained on all regions and
249 decoders trained on all-but-one region. Exclusion of any region resulted in decreased
250 performance ($p < 3e-4$, $n = 100$; Wilcoxon signed-rank test). Box plots as described in
251 Figure 2.
252

253 *Silently mimed speech decoding*

254 Finally, since future speech decoding applications must work even when speakers
255 do not produce audible sounds, we tested our decoder with a held-out set of 58 sentences
256 in which the participant (P1) audibly produced each sentence and then mimed the same
257 sentence, making the same kinematic movements but without making sound. Even
258 though the decoder was not trained on any mimed speech, the spectrograms of
259 synthesized silent speech demonstrated similar spectral features when compared to
260 synthesized audible speech of the same sentence (Figure 4a-c). After dynamic time
261 warping the acoustics of the decoded silent speech with the original audio of the
262 preceding audibly produced sentence, we calculated the spectral distortion and
263 correlation of the spectral features (Figure 4d,e). As expected, performance on mimed
264 speech was inferior to spoken speech (30% MCD difference) although this is consistent
265 with earlier work on silent facial EMG-to-speech synthesis where decoding performance
266 from EMG signals was significantly worse when participants silently articulated without
267 audible speech output²⁹. The performance gap may also be due to the absence of voicing
268 and laryngeal activation. This demonstrates that it is possible to decode important
269 spectral features of speech that were never audibly uttered ($p < 1e-11$, compared to
270 chance, $n = 58$; Wilcoxon signed-rank test).



272 **Figure 4: Speech synthesis from neural decoding of silently mimed speech. a-c,**
273 Spectrograms of original spoken sentence (a), neural decoding from audible production
274 (b), and neural decoding from silently mimed production (c). d, e, Spectral distortion
275 (MCD) (d) and correlation of original and decoded spectral features (e) for audibly and
276 silently produced speech. Since correlations are with respect to original audibly produced
277 sentences, decoded sentences that were silently mimed were dynamically time-warped
278 according to their spectral features. Decoded sentences were significantly better than
279 chance-level decoding for both speaking conditions ($p < 1e-11$, for all comparisons, $n =$
280 58; Wilcoxon signed-rank test). Box plots as described in Figure 2.
281

282 *Discussion*

283 Our results demonstrate intelligible speech synthesis from ECoG during both
284 audible and silently mimed speech production. Previous strategies for neural decoding of
285 speech have primarily focused on direct classification of speech segments like phonemes
286 or words^{30,31,32,33}. However, these demonstrations have been limited in their ability to
287 scale to larger vocabulary sizes and communication rates. Meanwhile, decoding of
288 auditory cortex responses has been more successful for continuous speech sounds^{18,34}, in
289 part because of the direct relationship between the auditory encoding of spectrotemporal
290 information and the reconstructed spectrogram. An outstanding question has been
291 whether decoding vocal tract movements from the speech motor cortex could be used for
292 generating high-fidelity acoustic output.

293 We believe that cortical activity at vSMC electrodes was critical for decoding
294 (Figure 3e,f) because it encodes the underlying articulatory physiology that produces
295 speech⁶. Our decoder explicitly incorporated this knowledge to simplify the complex
296 mapping from neural activity to sound by first decoding the physiological correlate of
297 neural activity and then transforming to speech acoustics. We have demonstrated that this
298 statistical mapping permits generalization with limited amounts of training.

299 Direct speech synthesis has several major advantages over spelling-based
300 approaches. In addition to the capability to communicate at a natural speaking rate, it
301 captures prosodic elements of speech that are not available with text output, for example
302 pitch intonation (Figure 2d) and word emphasis³⁵. Furthermore, a practical limitation for
303 current alternative communication devices is the cognitive effort required to learn and use
304 them. For patients in whom the cortical processing of articulation is still intact, a speech-
305 based BCI decoder may be far more intuitive and easier to learn to use^{14,15}.

306 Brain-computer interfaces are rapidly becoming clinically viable means to restore
307 lost function³⁶. Impressive gains have already been made motor restoration of cursor
308 control and limb movements. Neural prosthetic control was first demonstrated in
309 participants without disabilities^{37,38,39} before translating the technology to participants
310 with tetraplegia^{40,41,42,43}. While this articulatory-based approach establishes a new
311 foundation for speech decoding, we anticipate additional improvements from modeling
312 higher-order linguistic and planning goals^{44,45}. Our results may be an important next step
313 in realizing speech restoration for patients with paralysis.

314

315

316

317

318 **Methods**

319

320 **Participants and experimental task.** Three human participants (30 F, 31 F, 34 M)
321 underwent chronic implantation of high-density, subdural electrode array over the lateral
322 surface of the brain as part of their clinical treatment of epilepsy (right, left, and right
323 hemisphere grids, respectively). Participants gave their written informed consent before
324 the day of the surgery. All participants were fluent in English. All protocols were
325 approved by the Committee on Human Research at UCSF. Each participant read and/or
326 freely spoke a variety of sentences. P1 read aloud two complete sets of 460 sentences
327 from the MOCHA-TIMIT database⁴⁶. Additionally, P1 also read aloud passages from the
328 following stories: Sleeping Beauty, Frog Prince, Hare and the Tortoise, The Princess and
329 the Pea, and Alice in Wonderland. P2 read aloud one full set of 460 sentences from the
330 MOCHA-TIMIT database and further read a subset of 50 sentences an additional 9 times
331 each. P3 read 596 sentences describing three picture scenes and then freely described the
332 seen resulting in another 254 sentences. P3 also spoke 743 sentences during free response
333 interviews. In addition to audible speech, P1 also read 10 sentences 12 times each
334 alternating between audible and silent (mimed i.e. making the necessary mouth
335 movements) speech. Microphone recordings were obtained synchronously with the ECoG
336 recordings.

337

338 **Data acquisition and signal processing.** Electroencephalography was recorded with a
339 multi-channel amplifier optically connected to a digital signal processor (Tucker-Davis
340 Technologies). Speech was amplified digitally and recorded with a microphone

341 simultaneously with the cortical recordings. ECoG electrodes were arranged in a 16 x 16
342 grid with 4 mm pitch. The grid placements were decided upon purely by clinical
343 considerations. ECoG signals were recorded at a sampling rate of 3,052 Hz. Each channel
344 was visually and quantitatively inspected for artifacts or excessive noise (typically 60 Hz
345 line noise). The analytic amplitude of the high-gamma frequency component of the local
346 field potentials (70 - 200 Hz) was extracted with the Hilbert transform and down-sampled
347 to 200 Hz. The low frequency component (1-30 Hz) was also extracted with a 5th order
348 Butterworth bandpass filter and parallelly aligned with the high-gamma amplitude.
349 Finally, the signals were z-scored relative to a 30 second window of running mean and
350 standard deviation, so as to normalize the data across different recording sessions. We
351 studied high-gamma amplitude because it has been shown to correlate well with multi-
352 unit firing rates and has the temporal resolution to resolve fine articulatory movements¹⁷.
353 We also included a low frequency signal component due to the decoding performance
354 improvements note for reconstructing perceived speech from auditory cortex³⁴. Decoding
355 models were constructed using all electrodes from vSMC, STG, and IFG except for
356 electrodes with bad signal quality as determined by visual inspection.

357

358 **Phonetic and phonological transcription.** For the collected speech acoustic recordings,
359 transcriptions were corrected manually at the word level so that the transcript reflected
360 the vocalization that the participant actually produced. Given sentence level
361 transcriptions and acoustic utterances chunked at the sentence level, hidden Markov
362 model based acoustic models were built for each participant so as to perform sub-

363 phonetic alignment⁴⁷. Phonological context features were also generated from the
364 phonetic labels, given their phonetic, syllabic and word contexts.

365

366 **Cortical surface extraction and electrode visualization.** We localized electrodes on
367 each individual's brain by co-registering the preoperative T1 MRI with a postoperative
368 CT scan containing the electrode locations, using a normalized mutual information
369 routine in SPM12. Pial surface reconstructions were created using Freesurfer. Final
370 anatomical labeling and plotting was performed using the `img_pipe` python package⁴⁸.

371

372 **Inference of articulatory kinematics.** The articulatory kinematics inference model
373 comprises a stacked deep encoder-decoder, where the encoder combines phonological
374 and acoustic representations into a latent articulatory representation that is then decoded
375 to reconstruct the original acoustic signal. The latent representation is initialized with
376 inferred articulatory movement from Electromagnetic Midsagittal Articulography
377 (EMA)⁶ and appropriate manner features.

378 Chartier et al., 2018 described a statistical subject-independent approach to
379 acoustic-to-articulatory inversion which estimates 12 dimensional articulatory kinematic
380 trajectories (x and y displacements of tongue dorsum, tongue blade, tongue tip, jaw,
381 upper lip and lower lip, as would be measured by EMA) using only the produced
382 acoustics and phonetic transcriptions. Since, EMA features do not describe all
383 acoustically consequential movements of the vocal tract, we append complementary
384 speech features that improve reconstruction of original speech. In addition to voicing and
385 intensity of the speech signal, we added place manner tuples (represented as continuous

386 binary valued features) to bootstrap the EMA with what we determined were missing
387 physiological aspects in EMA. There were 18 additional values to capture the following
388 place-manner tuples: 1) velar stop, 2) velar nasal, 3) palatal approximant, 4) palatal
389 fricative, 5) palatal affricate, 6) labial stop, 7) labial approximant, 8) labial nasal, 9)
390 glottal fricative, 10) dental fricative, 11) labiodental fricative, 12) alveolar stop, 13)
391 alveolar approximant, 14) alveolar nasal, 15) alveolar lateral, 16) alveolar fricative, 17)
392 unconstructed, 18) voicing. For this purpose, we used an existing annotated speech
393 database (Wall Street Journal Corpus)⁴⁹ and trained speaker independent deep recurrent
394 network regression models to predict these place-manner vectors only from the acoustics,
395 represented as 25-dimensional Mel Frequency Cepstral Coefficients (MFCCs). The
396 phonetic labels were used to determine the ground truth values for these labels (e.g., the
397 dimension “labial stop” would be 1 for all frames of speech that belong to the phonemes
398 /p/, /b/ and so forth). However, with a regression output layer, predicted values were not
399 constrained to the binary nature of the input features. In all, these 32 combined feature
400 vectors form the initial articulatory feature estimates.

401 Finally, to ensure that the combined 32 dimensional representation has the
402 potential to reliably reconstruct speech, we designed an autoencoder to optimize these
403 values. Specifically, a recurrent neural network encoder is trained to convert
404 phonological and acoustic features to the initialized 32 articulatory representations and
405 then a decoder converts the articulatory representation back to the acoustics. The stacked
406 network is re-trained optimizing the joint loss on acoustic and EMA parameters. After
407 convergence, the encoder is used to estimate the final articulatory kinematic features that
408 act as the intermediate to decode acoustics from ECoG.

409

410 **Neural decoder.** The decoder maps ECoG recordings to MFCCs via a two stage process
411 by learning intermediate mappings between ECoG recordings and articulatory kinematic
412 features, and between articulatory kinematic features and acoustic features. We
413 implemented this model using TensorFlow in python⁵⁰. In the first stage, a stacked 3-
414 layer bLSTM¹⁶ learns the mapping between 300 ms windows of high-gamma and LFP
415 signals and the corresponding single time point of the 32 articulatory features. In the
416 second stage, an additional stacked 3-layer learns the mapping between the output of the
417 first stage (decoded articulatory features) and 32 acoustic parameters for full sentences
418 sequences. These parameters are 25 dimensional MFCCs, 5 sub-band voicing
419 strengths for glottal excitation modelling, $\log(F_0)$, voicing. At each stage, the model is
420 trained to with a learning rate of 0.001 to minimize mean-squared error of the target.
421 Dropout rate is set to 50% to suppress overfitting tendencies of the model. We use a
422 bLSTM because of their ability to retain temporally distant dependencies when
423 decoding a sequence⁵¹.

424

425 **Speech synthesis from acoustic features.** We used an implementation of the Mel-log
426 spectral approximation algorithm with mixed excitation²² to generate the speech
427 waveforms from estimates of the MFCCs from the neural decoder.

428

429 **Model training procedure.** As described, simultaneous recordings of ECoG and speech
430 are collected in short blocks of approximately 5 minutes. To partition the data for model
431 development, we allocated 2-3 blocks for model testing, 1 block for model optimization,

432 and the remaining blocks for model training. The test sentences for P1 and P2 each
433 spanned 2 recording blocks and comprised 100 sentences read aloud. The test sentences
434 for P3 were different because the speech comprised 100 sentences over three blocks of
435 freely and spontaneously speech describing picture scenes.

436 For shuffling the data to test for significance, we shuffled the order of the
437 electrodes that were fed into the decoder. This method of shuffling preserved the
438 temporal structure of the neural activity.

439

440 **Mel-Cepstral Distortion (MCD).** To examine the quality of synthesized speech, we
441 calculated the Mel-Cepstral Distortion (MCD) of the synthesized speech when compared
442 the original ground-truth audio. MCD is an objective measure of error determined from
443 MFCCs and is correlated to subjective perceptual judgements of acoustic quality²². For
444 reference acoustic features $mc^{(y)}$ and decoded features $mc^{(\hat{y})}$,

445

$$MCD = \frac{10}{\ln(10)} \sqrt{\sum_{0 < a < 25} (mc_a^{(y)} - mc_a^{(\hat{y})})^2}$$

446

447 **Intelligibility Assessment.** Listening tests using crowdsourcing are a standard way of
448 evaluating the perceptual quality of synthetic speech⁵². We used the Amazon Mechanical
449 Turk to assess the intelligibility of the neurally synthesized speech samples. We set up a
450 listening task where naïve listeners identified which of 10 sentences was played in each
451 trial. A set of 60 sentences (6 trials of 10 unique sentences) were evaluated in this
452 assessment. These trials, also held out during training the decoder, were used in place of

453 the 100 unique sentences tested throughout the rest of Figure 2 because the listeners
454 always had the same 10 sentences to chose from. Each trial sentence was listened to by
455 50 different listeners. In all, 166 unique listeners took part in the evaluations.

456

457 **Data limitation analysis.** To assess the amount of training data affects decoder
458 performance, we partitioned the data by recording blocks and trained a separate model for
459 an allotted number of blocks. In total, 8 models were trained, each with one of the
460 following block allotments: [1, 2, 5, 10, 15, 20, 25, 28]. Each block comprised an average
461 of 50 sentences recorded in one continuous session.

462

463 **Quantification of silent speech synthesis.** By definition, there was no acoustic signal to
464 compare the decoded silent speech. In order to assess decoding performance, we
465 evaluated decoded silent speech in regards to the audible speech of the same sentence
466 uttered immediately prior to the silent trial. We did so by dynamically time warping⁵³ the
467 decoded silent speech MFCCs to the MFCCs of the audible condition and computing
468 Pearson's correlation coefficient and Mel-cepstral distortion.

469

470 **Phoneme acoustic similarity analysis.** We compared the acoustic properties of decoded
471 phonemes to ground-truth to better understand the performance of our decoder. To do
472 this, we sliced all time points for which a given phoneme was being uttered and used the
473 corresponding time slices to estimate its distribution of spectral properties. With principal
474 components analysis (PCA), the 32 spectral features were projected onto the first 4
475 principal components before fitting the gaussian kernel density estimate (KDE) model.

476 This process was repeated so that each phoneme had two KDEs representing either its
477 decoded and or ground-truth spectral properties. Using Kullback-Leibler divergence (KL
478 divergence), we compared each decoded phoneme KDE to every ground-truth phoneme
479 KDE, creating an analog to a confusion matrix used in discrete classification decoders.
480 KL divergence provides a metric of how similar two distributions are to one another by
481 calculating how much information is lost when we approximate one distribution with
482 another. Lastly, we used Ward's method for agglomerative hierarchical clustering to
483 organize the phoneme similarity matrix.

484

485

486

487

488

489

490 **References:**

491

492 1. Wolpaw, J. R., Birbaumer, N., McFarland, D. J., Pfurtscheller, G., & Vaughan, T.
493 M. (2002). Brain–computer interfaces for communication and control. *Clinical*
494 *neurophysiology*, 113(6), 767-791.

495 2. Herff, C., & Schultz, T. (2016). Automatic Speech Recognition from Neural
496 Signals : A Focused Review, 10(September), 1–7.
497 <https://doi.org/10.3389/fnins.2016.00429>

498 3. Bocquelet F, Hueber T, Girin L, Chabardès S, Yvert B. (2016). Key
499 considerations in designing a speech brain computer interface. *J Physiol Paris*,
500 110: 392-401.

501 4. Brumberg, J. S., Pitt, K. M., Mantie-Kozlowski, A., & Burnison, J. D. (2018).
502 Brain–Computer Interfaces for Augmentative and Alternative Communication: A
503 Tutorial. *American journal of speech-language pathology*, 27(1), 1-12.

504 5. Lotte, F., Brumberg, J. S., Brunner, P., Gunduz, A., Ritaccio, A. L., Guan, C., &
505 Schalk, G. (2015). Electrographic representations of segmental features in
506 continuous speech. *Frontiers in human neuroscience*, 9, 97.

507 6. Chartier, J., Anumanchipalli, G. K., Johnson, K., & Chang, E. F. (2018).
508 Encoding of Articulatory Kinematic Trajectories in Human Speech Sensorimotor
509 Cortex. *Neuron*, 98(5), 1042–1054.e4.
510 <https://doi.org/10.1016/j.neuron.2018.04.031>

511 7. Majaranta, P., & Rähkä, K. J. (2002, March). Twenty years of eye typing: systems
512 and design issues. In *Proceedings of the 2002 symposium on Eye tracking*
513 *research & applications* (pp. 15-22). ACM.

514 8. Farwell, L. A., & Donchin, E. (1988). Talking off the top of your head: toward a
515 mental prosthesis utilizing event-related brain potentials. *Electroencephalography*
516 *and clinical Neurophysiology*, 70(6), 510-523.

517 9. Pandarinath, C., Nuyujukian, P., Blabe, C. H., Sorice, B. L., Saab, J., Willett, F.
518 R., ... Henderson, J. M. (2017). High performance communication by people with
519 paralysis using an intracortical brain-computer interface. *ELife*, 6, 1–27.
520 <https://doi.org/10.7554/eLife.18554>

521 10. Guenther, F. H., Brumberg, J. S., Joseph Wright, E., Nieto-Castanon, A.,
522 Tourville, J. A., Panko, M., ... Kennedy, P. R. (2009). A wireless brain-machine
523 interface for real-time speech synthesis. *PLoS ONE*, 4(12).
524 <https://doi.org/10.1371/journal.pone.0008218>

- 525 11. Newell, A., Langer, S., & Hickey, M. (1998). The rôle of natural language
526 processing in alternative and augmentative communication. *Natural Language*
527 *Engineering*, 4(1), 1-16.
- 528 12. Bocquelet, F., Hueber, T., Girin, L., Savariaux, C., & Yvert, B. (2016). Real-time
529 control of an articulatory-based speech synthesizer for brain computer
530 interfaces. *PLoS computational biology*, 12(11), e1005119.
- 531 13. Browman, C. P., & Goldstein, L. (1992). Articulatory phonology: An overview.
532 *Phonetica*, 49(3-4), 155-180.
- 533 14. Sadtler, P. T., Quick, K. M., Golub, M. D., Chase, S. M., Ryu, S. I., Tyler-Kabara,
534 E. C., ... & Batista, A. P. (2014). Neural constraints on
535 learning. *Nature*, 512(7515), 423.
- 536 15. Golub, M. D., Sadtler, P. T., Oby, E. R., Quick, K. M., Ryu, S. I., Tyler-Kabara,
537 E. C., ... & Yu, B. M. (2018). Learning by neural reassociation. *Nat. Neurosci.*,
538 21.
- 539 16. Graves, A., & Schmidhuber, J. (2005). Framewise phoneme classification with
540 bidirectional LSTM and other neural network architectures. *Neural Networks*,
541 18(5-6), 602-610.
- 542 17. Crone, N.E., Hao, L., Hart, J., Jr., Boatman, D., Lesser, R.P., Irizarry, R., and
543 Gordon, B. (2001). Electrographic gamma activity during word production
544 in spoken and sign language. *Neurology* 57, 2045–2053.
- 545 18. Akbari H., Khalighinejad B., Herrero J., Mehta A., Mesgarani N. (2018)
546 Reconstructing intelligible speech from the human auditory cortex. bioRxiv
547 350124; doi: <https://doi.org/10.1101/350124>
- 548 19. Bouchard, K.E., Mesgarani, N., Johnson, K., and Chang, E.F. (2013). Functional
549 organization of human sensorimotor cortex for speech articulation. *Nature* 495,
550 327–332.
- 551 20. Mesgarani, N., Cheung, C., Johnson, K., & Chang, E. F. (2014). Phonetic feature
552 encoding in human superior temporal gyrus. *Science*, 343(6174), 1006-1010.
- 553 21. Flinker, A., Korzeniewska, A., Shestyuk, A. Y., Franaszczuk, P. J., Dronkers, N.
554 F., Knight, R. T., & Crone, N. E. (2015). Redefining the role of Broca's area in
555 speech. *Proceedings of the National Academy of Sciences*, 112(9), 2871-2875.
- 556 22. Zheng, F., Zhang, G., & Song, Z. (2001). Comparison of different
557 implementations of MFCC. *Journal of Computer science and Technology*, 16(6),
558 582-589.

- 559 23. Yoshimura, T., Tokuda, K., Masuko, T., Kobayashi, T., & Kitamura, T., (2001).
560 Mixed excitation for HMM-based Speech Synthesis, Eurospeech 2001.
- 561 24. Davis, S. B., & Mermelstein, P. (1990). Comparison of parametric representations
562 for monosyllabic word recognition in continuously spoken sentences. In Readings
563 in speech recognition (pp. 65-74).
- 564 25. Janke, M. and Diener, L. (2017). EMG-to-Speech: Direct Generation of Speech
565 From Facial Electromyographic Signals. IEEE/ACM Trans. Audio, Speech and
566 Lang. Proc. 25, 12 (December 2017), 2375-2385. DOI:
567 <https://doi.org/10.1109/TASLP.2017.2738568>
- 568 26. Drullman, R., Festen, J. M. & Plomp, R. Effect of temporal envelope smearing on
569 speech reception. J. Acoust. Soc. Am. 95, 1053–1064 (1994).
- 570 27. Shen, Jonathan et. al., (2018) Natural TTS by conditioning Wavenet on Mel-
571 spectrogram predictions. In proceedings of ICASSP 2018,
572 <https://arxiv.org/abs/1712.05884>
- 573 28. Kominek, J., Schultz, T., and Black, A. (2008). "Synthesizer voice quality of new
574 languages calibrated with mean mel cepstral distortion", In *SLTU-2008*, 63-68.
- 575 29. Janke, M. (2016). EMG-to-Speech: Direct Generation of Speech from facial
576 Electromyographic Signals. PhD Dissertation, Karlsruhe Institute of
577 Technology, Germany, 2016
- 578 30. Mugler, E.M., Patton, J.L., Flint, R.D., Wright, Z.A., Schuele, S.U., Rosenow, J.,
579 Shih, J.J., Krusienski, D.J., and Slutzky, M.W. (2014). Direct classification of all
580 American English phonemes using signals from functional speech motor cortex. J.
581 Neural Eng. 11, 035015.
- 582 31. Herff, C., Heger, D., de Pestors, A., Telaar, D., Brunner, P., Schalk, G., and
583 Schultz, T. (2015). Brain-to-text: decoding spoken phrases from phone
584 representations in the brain.
- 585 32. Moses, D. A., Mesgarani, N., Leonard, M. K., & Chang, E. F. (2016). Neural
586 speech recognition: continuous phoneme decoding using spatiotemporal
587 representations of human cortical activity. Journal of neural engineering, 13(5),
588 056004.
- 589 33. Livezey, J. A., Bouchard, K. E., & Chang, E. F. (2018). Deep learning as a tool
590 for neural data analysis: speech classification and cross-frequency coupling in
591 human sensorimotor cortex. arXiv preprint arXiv:1803.09807.

- 592 34. Pasley, B. N., David, S. V, Mesgarani, N., Flinker, A., & Shamma, S. A. (2012).
593 Reconstructing Speech from Human Auditory Cortex. *PLoS Biol*, 10(1), 1001251.
594 <https://doi.org/10.1371/journal.pbio.1001251>
- 595 35. Dichter B. K., Breshears J. D., Leonard M. K., and Chang E. F. (2018) The
596 Control of Vocal Pitch in Human Laryngeal Motor Cortex. *Cell*, 174, 21–31
- 597 36. Leuthardt, E. C., Schalk, G., Moran, D., & Ojemann, J. G. (2006). The emerging
598 world of motor neuroprosthetics: a neurosurgical perspective.
599 *Neurosurgery*, 59(1), 1.
- 600 37. Wessberg J, Stambaugh CR, Kralik JD, Beck PD, Laubach M, et al. (2000) Real-
601 time prediction of hand trajectory by ensembles of cortical neurons in primates.
602 *Nature* 408: 361–365.
- 603 38. Serruya MD, Hatsopoulos NG, Paninski L, Fellows MR, Donoghue JP (2002)
604 Instant neural control of a movement signal. *Nature* 416: 141–142.
- 605 39. Taylor DM, Tillery SI, Schwartz AB (2002) Direct cortical control of 3D
606 neuroprosthetic devices. *Science* 296: 1829–1832.
- 607 40. Hochberg, L. R., Serruya, M. D., Friehs, G. M., Mukand, J. A., Saleh, M., Caplan,
608 A. H., ... & Donoghue, J. P. (2006). Neuronal ensemble control of prosthetic
609 devices by a human with tetraplegia. *Nature*, 442(7099), 164
- 610 41. Collinger, J. L., Wodlinger, B., Downey, J. E., Wang, W., Tyler-Kabara, E. C.,
611 Weber, D. J., ... & Schwartz, A. B. (2013). High-performance neuroprosthetic
612 control by an individual with tetraplegia. *The Lancet*, 381(9866), 557-564.
- 613 42. Aflalo, T., Kellis, S., Klaes, C., Lee, B., Shi, Y., Pejsa, K., ... & Andersen R. A.
614 (2015). Decoding motor imagery from the posterior parietal cortex of a tetraplegic
615 human. *Science*, 348(6237), 906-910.
- 616 43. Ajiboye, A. B., Willett, F. R., Young, D. R., Memberg, W. D., Murphy, B. A.,
617 Miller, J. P., ... & Peckham, P. H. (2017). Restoration of reaching and grasping
618 movements through brain-controlled muscle stimulation in a person with
619 tetraplegia: a proof-of-concept demonstration. *The Lancet*, 389(10081), 1821-
620 1830.
- 621 44. Snyder, L. H., Batista, A. P., Andersen, R. A., (1997) Coding of intention in the
622 posterior parietal cortex, *Nature* 386, 167-170, 1997

623 45. Huth, A. G., de Heer, W. A., Griffiths, T. L., Theunissen, F. E., & Gallant, J. L.
624 (2016). Natural speech reveals the semantic maps that tile human cerebral
625 cortex. *Nature*, 532(7600), 453.

626 **Method References**

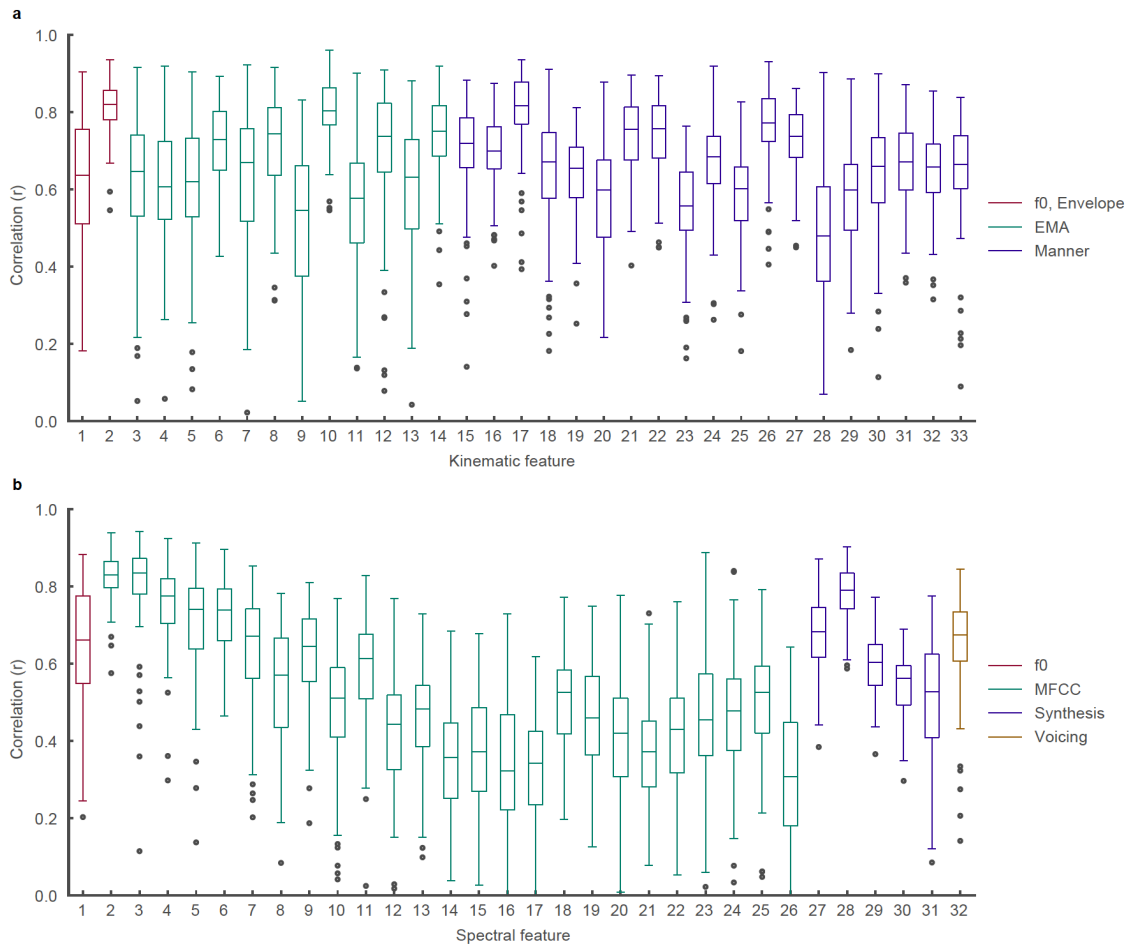
- 627 46. Wrench, A. (1999). MOCHA: multichannel articulatory database.
628 <http://www.cstr.ed.ac.uk/research/projects/artic/mocha.html>.
- 629 47. Prahallad, K., Black, A.W., and Mosur, R. (2006). Sub-phonetic modeling for
630 capturing pronunciation variations for conversational speech synthesis. In
631 Proceedings of the 2006 IEEE International Conference on Acoustics Speech and
632 Signal Processing (ICASSP), pp. I–I.
- 633 48. Hamilton, L. S., Chang, D. L., Lee, M. B., & Chang, E. F. (2017). Semi-
634 automated Anatomical Labeling and Inter-subject Warping of High-Density
635 Intracranial Recording Electrodes in Electrocortigraphy. *Frontiers in*
636 *Neuroinformatics*, 11, 62. <http://doi.org/10.3389/fninf.2017.00062>
- 637 49. Paul, B., D, and Baker, M., J, (1992). The design for the wall street journal-based
638 CSR corpus. In Proceedings of the workshop on Speech and Natural Language
639 (HLT '91). Association for Computational Linguistics, Stroudsburg, PA, USA,
640 357-362. DOI: <https://doi.org/10.3115/1075527.1075614>
- 641 50. Martín Abadi, Ashish Agarwal, Paul Barham, Eugene Brevdo, Zhifeng Chen, et
642 al. (2015). TensorFlow: Large-scale machine learning on heterogeneous systems.
643 <http://www.tensorflow.org>
- 644 51. Hochreiter, S., and Schmidhuber, J. (1997). Long short-term memory. *Neural*
645 *Comput.* 9, 1735-1780.
- 646 52. Wolters, M. K., Isaac, Renals, S., Evaluating Speech Synthesis intelligibility
647 using Amazon Mechanical Turk. (2010) In proceedings of ISCA speech synthesis
648 workshop (SSW7), 2010.
- 649 53. Berndt, D. J., & Clifford, J. (1994). Using dynamic time warping to find
650 patterns in time series. In KDD workshop (Vol. 10, No. 16, pp. 359-370).

651

652

653

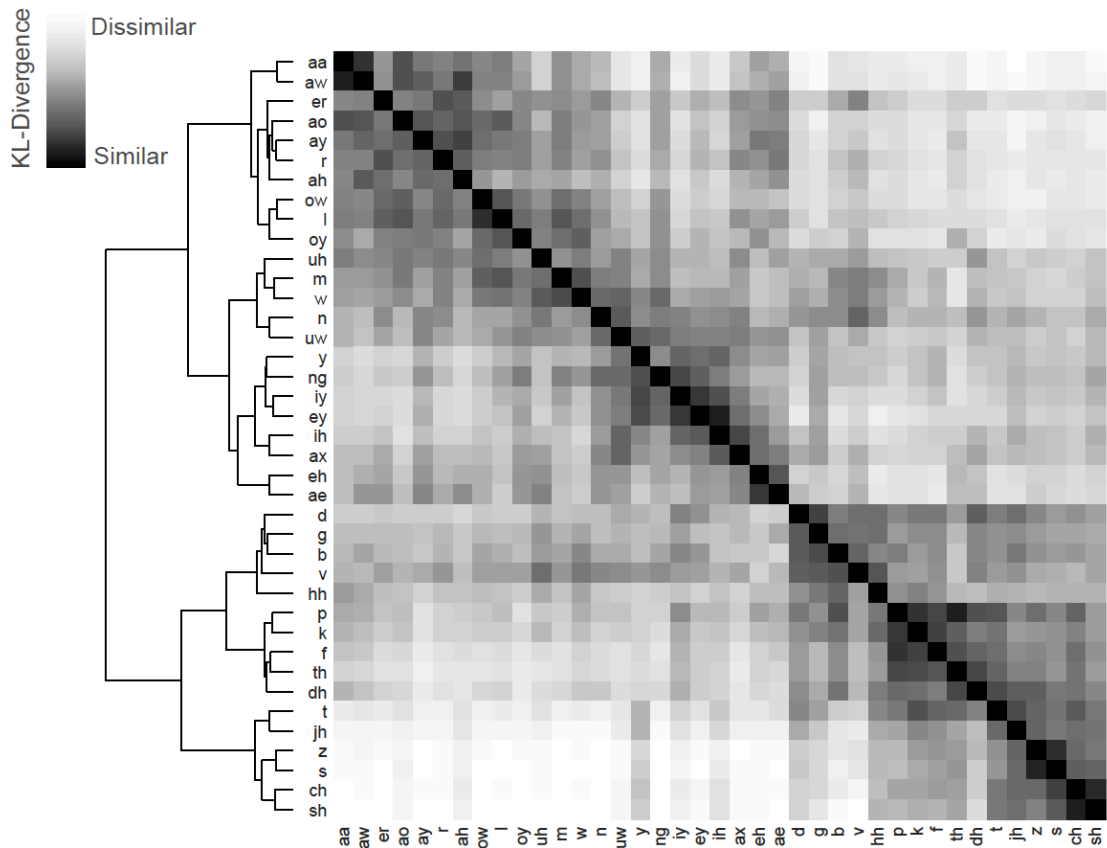
654 **Extended Data:**



655

656 **Extended Data Figure 1: Decoding performance of kinematic and spectral features.**

657 **a**, Correlations of all 33 decoded articulatory kinematic features with ground-truth. EMA
658 features represent X and Y coordinate traces of articulators (lips, jaw, and three points of
659 the tongue) along the midsagittal plane of the vocal tract. Manner features represent
660 complementary kinematic features to EMA that further describe acoustically
661 consequential movements. **b**, Correlations of all 32 decoded spectral features with
662 ground-truth. MFCC features are 25 mel-frequency cepstral coefficients that describe
663 power in perceptually relevant frequency bands. Synthesis features describe glottal
664 excitation weights necessary for speech synthesis.



665

666 **Extended Data Figure 2: Ground-truth acoustic similarity matrix.** Compares acoustic
667 properties of ground-truth spoken phonemes with one another. Similarity is computed by
668 first estimating a gaussian kernel density for each phoneme and then computing the
669 Kullback-Leibler (KL) divergence between a pair of a phoneme distributions. Each row
670 compares the acoustic properties of a two ground-truth spoken phonemes. Hierarchical
671 clustering was performed on the resulting similarity matrix.

672

673 **Acknowledgments**

674 We thank Matthew Leonard, Neal Fox for their helpful comments on the manuscript. We
675 also thank Ben Speidel for his work reconstructing MRI images of patients' brains. This

676 work was supported by grants from the NIH (DP2 OD008627 and U01 NS098971-01).

677 E.F.C is a New York Stem Cell Foundation- Robertson Investigator. This research was

678 also supported by The New York Stem Cell Foundation, the Howard Hughes Medical

679 Institute, The McKnight Foundation, The Shurl and Kay Curci Foundation, and The

680 William K. Bowes Foundation.

681

682 **Author Contributions** Conception G.K.A., J.C., and E.F.C.; Articulatory kinematics

683 inference G.K.A; Decoder design G.K.A and J.C.; Decoder analyses: J.C.; Data

684 collection G.K.A., E.F.C., and J.C.; Prepared manuscript all; Project Supervision E.F.C.

685

686